ACS Synthetic Biology
Cite This: ACS Synth. Biol. 2019, 8, 264−273
Letter
pubs.acs.org/synthbio

A Regulatory NADH/NAD+ Redox Biosensor for Bacteria

Yang Liu,[†,§] Robert Landick,[†,‡,§] and Srivatsan Raman*[,†,‡,§]

[†]Department of Biochemistry, [‡]Department of Bacteriology, and [§]The Great Lakes Bioenergy Research Center, University of Wisconsin-Madison, Madison, Wisconsin 53706, United States

Supporting Information

ABSTRACT: NADH and NAD+ cofactors drive hundreds of biochemical reactions, and their ratio is a key metabolic marker of cellular state. Traditional assays to measure the NADH/NAD+ ratio is laborious, prone to inaccuracies, and not suitable for high-throughput screening. We report a genetically encoded ratiometric biosensor for NADH/NAD+ based on redox-responsive bacterial transcription factor Rex that overcomes these limitations. We engineered a Rex-regulated *E. coli* promoter with improved biosensor characteristics by tuning the affinity of Rex and the operator site. Since NADH is oxidized during aerobic respiration, we used the biosensor-reporter to investigate the effect of removing respiratory chain enzymes on NADH/NAD+ ratio during aerobiosis. We found that the NADH/NAD+ signal increased in five of the nine mutants by over 3-fold compared to wildtype, including an NADH dehydrogenase double mutant with 6-fold elevation. We also found that among several common carbon sources, *E. coli* grown on acetate exhibited higher NADH/NAD+ compared to *E. coli* grown on glucose. As a proof-of-concept for high-throughput redox screening, we were able to enrich high NADH mutants present at 1 in 10 000 among wildtype cells by biosensor-guided pooled screen. Thus, our Rex biosensor-reporter enables facile, noninvasive, high-throughput redox measurement to understand and engineer redox metabolism.

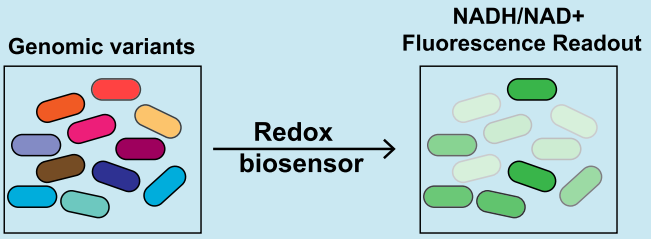

KEYWORDS: *redox biosensor, NADH/NAD+, high-throughput screening, bacterial physiology, respiratory chain*

Prokaryotic and eukaryotic cells use NAD(H) as a major electron carrier to power hundreds of essential redox reactions, and to directly or indirectly regulate biochemical processes, such as enzyme allostery and post-translational modifications.[1−3] NAD(H) is highly connected in the metabolic network, and even small perturbations to the NADH/NAD+ ratio can propagate widely across cellular processes. Because NAD(H) is an important metabolic marker, observing differences in redox can help distinguish normal vs diseased cells, estimate chemical potential within different organelles, and identify cell cycle states. In humans, abnormalities caused by imbalance of NADH/NAD$^+$ have been implicated in aging, diabetes, epilepsy, and cancer.[1,4] In bacteria, NADH/NAD$^+$ metabolism plays a key role in adaptability to an environment, and community structure.

E. coli has served as an excellent model system to elucidate the basic biology of the redox state. Glucose oxidation reduces NAD$^+$ to NADH through glycolysis and the TCA cycle. To maintain redox balance for cell survival, NADH is oxidized back to NAD$^+$. Anaerobically grown *E. coli* regenerates NAD$^+$ through many fermentative pathways by reducing metabolic intermediates such as pyruvate with NADH when no other electron acceptors (e.g., nitrate) are present.[5] Under aerobic conditions, *E. coli* utilizes the respiratory chain to oxidize NADH to NAD$^+$, and channels the redox energy to generate a proton gradient for ATP synthesis. The *E. coli* aerobic respiratory chain contains two NADH dehydrogenases (Ndh-I and Ndh-II) and three cytochrome oxidases (Cyt-bo3, Cyt-bd-I, and Cyt-bd-II). Genetic and biochemical characterization of these enzyme complexes suggest that they function under different physiological conditions.[6−10] However, the contribution of aerobic respiratory chain components toward NAD(H) metabolism has not been systematically and quantitatively characterized. The impact of removing respiratory chain enzymes on the NADH/NAD$^+$ ratio is poorly understood due to redundancies and compensatory roles among them. A broad goal is to gain a systems-level understanding of how deletions across the genome affect redox imbalance. Since the redox state is an emergent, global property that is affected by multiple metabolic pathways, a high-throughput genome-wide survey of genetic factors, beyond known candidates in central metabolism, would aid comprehensive understanding of determinants of the intracellular redox state.[11] Genome-wide redox screens are also useful in metabolic engineering for optimizing the redox state to drive new biosynthesis reactions.

The use of genetically encoded biosensors has revolutionized microbial genetics and biomanufacturing by enabling high-throughput screening of cellular phenotypes. A genetically encoded biosensor is usually an allosteric protein that upon binding to a target metabolite, undergoes chemical, conformational, or regulatory change coupled to a spectroscopic response. Since each cell is able to "self-report" the concentration of the metabolite, this approach can be scaled

Received: November 21, 2018
Published: January 11, 2019

DOI: 10.1021/acssynbio.8b00485
ACS Synth. Biol. 2019, 8, 264−273

to assay thousands of mutants that can be classified in a cell sorter based on the metabolite level. Biosensors exist for several common intracellular metabolites including calcium,[12] cyclic-GMP,[13] ATP,[14] and hydrogen peroxide.[15] In contrast, traditional techniques for measuring redox are low-throughput, lack accuracy, or both. Current NAD(H) quantification relies on NADH autofluorescence, enzymatic assays, or LC−MS (liquid chromatography coupled mass spectrometry).[16−18] These methods have three major drawbacks. First, the signal-to-noise is poor due to high background autofluorescence. Second, the measurement may be inaccurate owing to the unstable nature of NADH during sample preparation. Third, these assays are cumbersome and time-consuming, which limits the number of variant backgrounds or environmental conditions (*e.g.*, different carbon sources) that can be studied.

The objective of our study was to develop a genetically encoded biosensor for the NADH/NAD$^+$ ratio in bacteria to facilitate high-throughput redox screens. The sensor is based on Rex, an allosteric transcription factor that regulates gene expression by binding to NAD(H).[19−21] Rex undergoes a conformational change upon binding to NADH and several studies have taken advantage of this property of Rex to build NADH/NAD$^+$ biosensors by conformational coupling of a fluorescent protein to Rex.[22−24] Conformational coupling enables rapid response to NADH/NAD$^+$ changes, making these biosensors an excellent tool for imaging redox changes in real time. However, new conformational biosensors must be specifically engineered for different fluorescent reporters. For instance, current conformational biosensors engineered for oxygen-dependent fluorescent proteins[22−24] cannot be used in hypoxic or anaerobic conditions. Further, conformational biosensors are not suitable for regulation of engineered circuits in response to redox changes. Conformational biosensors have not been used for screening variant libraries, possibly due to a noisy or uneven signal at steady state. In contrast, regulatory biosensors can interface with endogenous pathways to control engineered circuits and have been widely used for screening large variant libraries in metabolic engineering.[25−29] Regulatory biosensors offer several advantages because they can transcriptionally control any gene of choice. Since transcription generates a steady signal, even if the physiology of the cell changes during screening, as it does while cell sorting, the reporter records the state of the cell when the reporter is expressed, and not when it is being read. This is particularly important because bacteria rapidly change redox levels when cells are not continuously exposed to oxygen. Further, a reporter can be chosen to suit experimental conditions (*e.g.*, aerobic vs anaerobic) or multiple reporters can be used simultaneously for different metabolites. Recently, yeast transcription factor Yap1p was repurposed as a regulatory redox biosensor in *S. cerevisiae* to select for *S. cerevisiae* variants with higher NADPH capacity.[30] However, to the best of our knowledge a regulatory NADH/NAD+ biosensor has not been implemented in bacteria to date.

In this study, we report a regulatory redox biosensor in *E. coli* for the NADH/NAD$^+$ ratio by porting Rex from *B. subtilis* (B-Rex) into *E. coli*. We functionalized B-Rex in *E. coli* by placing Rex operator sites with different affinities for B-Rex into a constitutive *E. coli* promoter. To compare different promoter designs, we evaluated biosensor-reporter activity in aerobic (low NADH) and anaerobic (high NADH) conditions, and chose an optimal design with good dynamic range and high reporter signal at full induction. To validate the reporter for future use in high-throughput screens, we applied the redox biosensor-reporter to investigate the functional contribution of aerobic respiratory chain enzymes on NADH/NAD$^+$ redox balance. We hypothesized that knocking out components in the respiratory chain pathway (NADH dehydrogenases and cytochrome oxidases) would abolish or attenuate NADH oxidation, leading to a buildup of NADH. We found that five of the nine single and double knock outs elevated NADH signal greater than 3-fold over wildtype *E. coli*. Highest NADH signal (6.1-fold increase) was measured in a strain in which both NADH dehydrogenases were disabled by the deletion of NADH dehydrogenase-II and the F-subunit of NADH dehydrogenase-I. Since the redox state can also be altered by changing the carbon source, we also tested NADH/NAD$^+$ of *E. coli* grown on several common carbon sources. We found that cells grown on acetate show nearly twice the NADH/NAD$^+$ signal as glucose, which is consistent with a previous metabolomics study.[16] We also demonstrated the utility of the Rex biosensor-reporter for high-throughput pooled screening by enriching high NADH cells at an abundance of 1 in 10 000 from a mixed population by fluorescence activated cell sorting.

RESULTS

Structure-Guided Analysis of Rex Operator Sites. We chose B-Rex for this study because it is biochemically and structurally well characterized with several known operator sites.[21] B-Rex binds to NADH and NAD+, but is only induced by NADH.[20,21] Thus, transcription from a B-Rex-regulated promoter is proportional to the NADH/NAD$^+$ ratio. To port B-Rex into *E. coli*, we modified a constitutive *E. coli* promoter to become B-Rex-responsive by inserting a B-Rex operator site after the transcription start site. Since B-Rex is a repressor, it would block RNA polymerase at low NADH by remaining bound to the operator. At high NADH, B-Rex dissociates from DNA to enable NADH-dependent gene regulation of a downstream fluorescent reporter. We preferred this strategy over using the native *B. subtilis* promoter because this approach can be adapted to port B-Rex to other nonmodel microbes and also allows us to tune biosensor properties in the absence of layered regulation embedded in native promoters. The choice of operator site was dictated by two biosensor properties—dynamic range and maximum reporter signal. Dynamic range is the ratio of reporter expression at high and low NADH. Maximum reporter signal is the absolute fluorescence units when a biosensor is fully induced. Both dynamic range and maximum reporter signal have to be large to accurately measure and resolve small redox differences between cells. High dynamic range improves signal-to-noise discrimination. High maximum reporter signal minimizes false positives from fluorescence-based cell sorting due to better sorting accuracy at higher signal intensities. However, maximizing one property can have an opposing effect on the other. If a biosensor has high affinity for an operator, then the dynamic range would be large due to the low baseline signal but the maximum reporter signal may be small. Alternatively, if a biosensor has low affinity for an operator, then the maximum reporter signal would be large but the dynamic range would be small due to high reporter baseline. Therefore, choosing an operator with the right binding affinity is essential for optimal biosensor-reporter activity.

There are seven known B-Rex operator sites (ROP) in *B. subtilis*, all sharing identical left half-sites, but with different

DOI: 10.1021/acssynbio.8b00485
ACS Synth. Biol. 2019, 8, 264−273

right half-sites.[21] We classified the ROPs into three groups: perfect, near-perfect, and imperfect palindromes (Figure 1A),

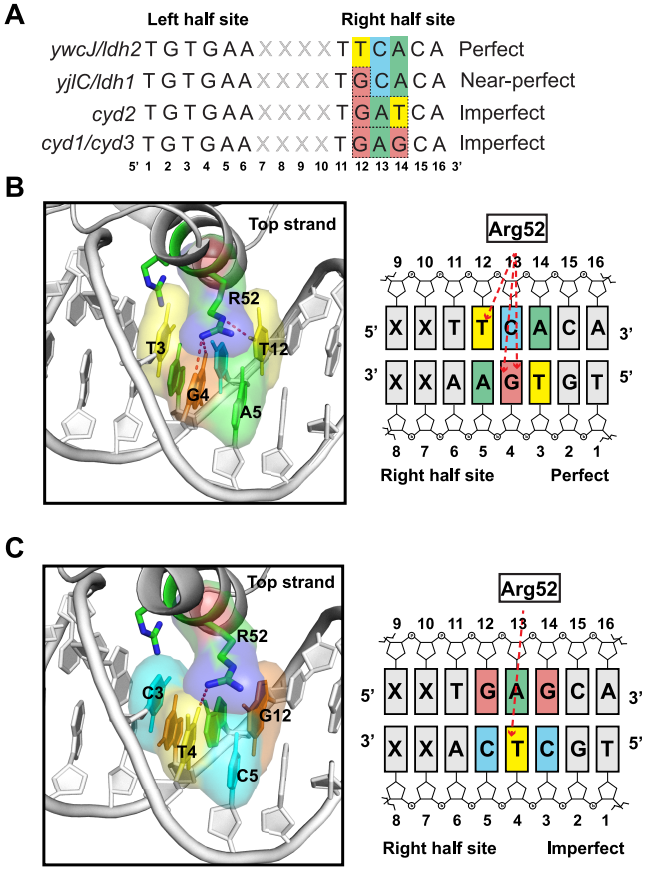

Figure 1. Structure and sequence analysis of B-Rex-operator site interactions. (A) Multiple sequence alignment of B-Rex operator sites from *B. subtilis*. Color shades mark bases that differ across operators and "X"s represent spacer between the half sites. (B) Structural model of interactions between major groove helix of B-Rex with the right half site of the perfect palindrome. B-Rex side chains modeled in T-Rex structure. (C) Structural model of interactions between major groove helix with the right half site of the imperfect palindrome. Dashed red lines represent hydrogen bonds between B-Rex and operator.

with the near-perfect and imperfect palindromes one and three bases away from a perfect palindrome, respectively. Differences between the ROPs were at base positions 12, 13, and 14 and in the spacer region between the half-sites (marked as 'X's in Figure 1A). Because it was unclear from sequence analysis alone which operator had the optimal affinity for B-Rex, we decided to test two ROPs with expected tighter and weaker binding. We took a structure-based approach to analyze interactions between the protein and DNA to choose suitable operators. The crystal structure of B-Rex is not complexed with DNA.[21] Therefore, we chose the DNA-bound structure of a close homologue from *Thermus aquaticus*, T-Rex, for analysis.[31] The DNA-binding domains of T-Rex and B-Rex share a sequence identity of 41% and a backbone root-mean square deviation of 1.24 Å. Six out of the 11 residues (T-Rex F43 to G53) along the major groove helix are identical to B-Rex, and the crucial DNA-contacting residues are conserved or similar (R46, K47 in T-Rex and R51, R52 in B-Rex, Supplementary Figure S1). The T-Rex-DNA structure shows that the spacer does not directly contact the protein backbone or side chains, and hence is not likely to contribute to binding. Since the left half-sites are identical, we focused our attention on the variant triplet (bases 12, 13, and 14) in the right half-site as the likely driver of binding affinity differences between operators. We modeled arginine at position 52 for B-Rex to replace the lysine at position 47 of T-Rex. Arg52 makes stronger interactions with the perfect palindrome than with the imperfect palindrome. In the perfect palindrome **TGTGAA**XXXX-**TTCACA**, Arg52 makes extensive hydrogen bonds with G4 and T12 in the right half site. Arg52 interacts with O6 and N7 of base G4, and O4 of base T12 (Figure 1B). Besides the hydrogen bonding interactions, Arg52 is also stabilized by hydrophobic interactions provided by bases T3 and T12. We chose the perfect palindrome (operator in 5′-UTR of *ywcJ* and *ldh2*) as the first candidate due to optimal protein−DNA contacts suggesting tight binding through hydrogen bonding, hydrophobic contacts, and stacking interactions. In the structural model of B-Rex with imperfect palindrome, **TGTGAAATATTGAGCA** (operator in 5′UTR of *cyd1*) modeled in by 3DNA, Arg52 loses two hydrogen bonds due to sequence changes (Figure 1C). Notably, the hydrophobic interactions provided by T3 and T12 in the perfect palindrome are significantly reduced in the imperfect palindrome (Figure 1C). This led us to conclude that the imperfect palindrome will likely have lower affinity for B-Rex than the perfect palindrome. We constructed two promoters: one embedded with the perfect palindrome **TGTGAA**ATAC**TTCACA** (ROP-PP) and another with an imperfect palindrome **TGTGAA**-ATAT**TGAGCA**, (ROP-IP). Both operators were inserted after the transcription start site on a medium strength, constitutive *E. coli* promoter, J23101, to generate promoter pROP-PP and pROP-IP.

Comparing the Performance of Promoter Designs under Aerobic vs Anaerobic Growth. We constructed a dual-plasmid system to evaluate the promoters. One plasmid constitutively expressed B-Rex (pB-Rex) and other carried a fluorescent reporter gene regulated either by pROP-PP or pROP-IP (Figure 2A). The biosensor-reporter system cannot be induced by exogenous NADH in the growth media because NADH is not permeable through the bacterial membrane. To induce the biosensor-reporter, we grew *E. coli* anaerobically since the NADH/NAD^+ ratio is higher in *E. coli* grown anaerobically than aerobically.[19] We independently validated this result using an enzyme-based commercial kit (see Materials and Methods). We evaluated the performance of ROP-PP and ROP-IP promoter designs by comparing reporter fluorescence of cells grown in aerobic (low NADH) vs anaerobic (high NADH) conditions. It is difficult to determine the dose−response function of the biosensor (*i.e.*, reporter fluorescence over a range of NADH/NAD^+ ratios) because the NAD(H) levels cannot be directly determined by exogenous supplementation in the growth media. However, we determine dynamic range and maximum reporter signal on the basis of end-point measurements. We used the FMN-based fluorescent protein (FbFP) as a reporter instead of GFP because FbFP is active in anaerobic conditions.[32] Cells constitutively expressing the reporter (no pB-Rex) had comparable fluorescence in aerobic and anaerobic conditions (Figure 2B,C, left bar of each set). This result suggested that promoter strength is the same under aerobic and anaerobic growth and that any differences in fluorescence observed when B-Rex is coexpressed were primarily dependent on B-Rex activity. It also established that the strength of the constitutive promoter was not impaired

DOI: 10.1021/acssynbio.8b00485
ACS Synth. Biol. 2019, 8, 264−273

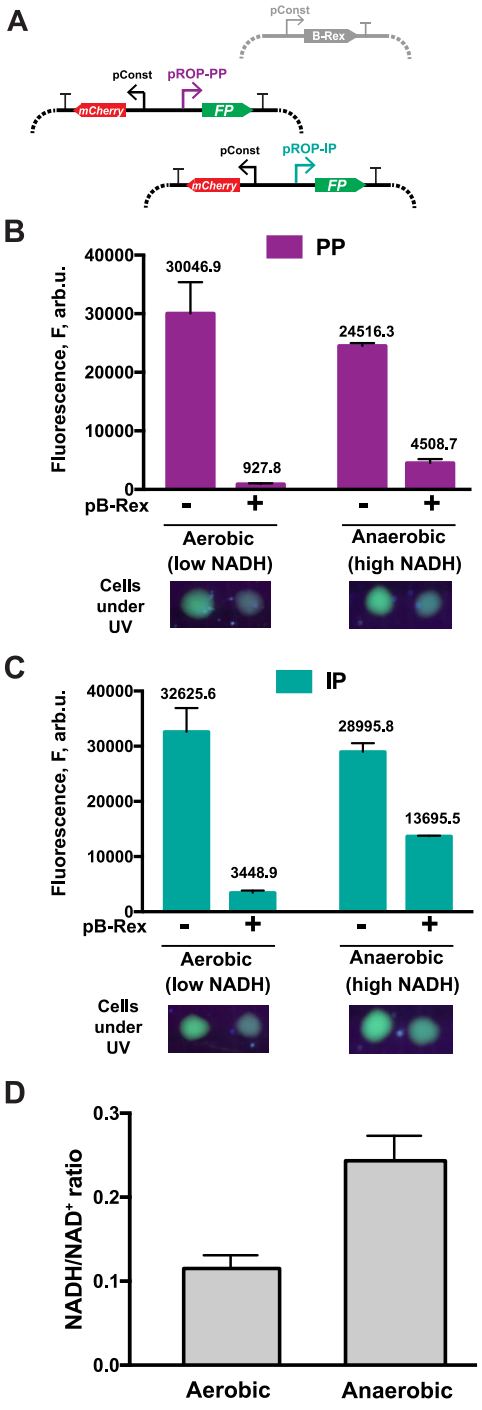

Figure 2. Comparison of redox biosensor-reporter activity of *E. coli* promoter embedded with Rex operators containing perfect (ROP-PP) and imperfect (ROP-IP) palindromes. (A) Schematic of the dual-plasmid system. Cells are transformed with pB-Rex expressing B-Rex from a constitutive *E. coli* promoter and reporter plasmids containing engineered promoters either pROP-PP (purple) or pROP-IP (cyan) driving expression of fluorescent protein (green arrow). (B and C) Biosensor properties of pROP-PP (B) and pROP-IP (C). pB-Rex- denotes cells constitutively expressing FbFP from an unregulated promoter at low and high NADH. pB-Rex+ denotes cells coexpressing B-Rex with corresponding promoters to regulate FbFP. Images below barchart shows culture under UV. (D) Kit based NAD(H) quantification for aerobic and anaerobic grown *E. coli*. *Y*-axis is normalized fluorescence units of FbFP. Error bar is standard deviation of three replicates.

by insertion of operator sites or from minor differences in ROP-PP and ROP-IP sequences. Under aerobic conditions (low NADH), when B-Rex was coexpressed, reporter fluorescence was diminished by 30- and 10-fold, respectively, in pROP-PP and pROP-IP containing cells (Figure 2B,C, compare "Aerobic" left and right bars). This result was consistent with our expectation that B-Rex should exert stronger repression by binding tighter to the perfect than the imperfect palindrome. Under anaerobic conditions (high NADH), both promoters were activated and their dynamic ranges, computed as the ratio of reporter fluorescence in anaerobic (high NADH) and aerobic (low NADH) conditions, were similar: pROP-PP, 4.9-fold and pROP-IP, 4.0-fold (Figure 2B,C, compare "Aerobic" and "Anaerobic" right bars). The enzyme-based assay independently confirms the redox change (Figure 2D). Maximum reporter signal at induction was well below constitutive reporter expression (Figure 2B,C, compare "Anaerobic" left and right bars) suggesting that the biosensor may not be saturated and that the physiological range of NADH/NAD^+ ratio under these growth conditions was within the detection range of both B-Rex promoter designs. Although the dynamic range of pROP-PP and pROP-IP promoters were similar, the induced reporter signal was much higher with pROP-IP than pROP-PP (13695 fluorescence units vs 4509 fluorescence units, Figures 2B,C). Therefore, we used ROP-IP system for further experiments in this study. We used GFP as the reporter in the following experiments as they were carried out under aerobic conditions.

Redox State in Respiratory Chain Mutants. NADH metabolism is closely linked to energy production due to its role in ATP synthesis. The *E. coli* respiratory chain comprises membrane-bound NADH dehydrogenases and cytochrome oxidases (Figure 3A). NADH dehydrogenases oxidize NADH and transfer electrons to quinones, which are subsequently oxidized by cytochrome oxidases passing electrons to the terminal electron acceptor O_2 to make H_2O. The respiratory chain converts energy stored in NADH to proton gradients, which can be used to power ATP synthesis (Figure 3A). In *E. coli*, there are two major NADH dehydrogenases, Ndh-I and Ndh-II. Ndh-I or NADH:ubiquinone oxidoreductase I (NuoA-N) is a multisubunit enzyme, which is similar in sequence to complex I of other bacteria, archaea, and eukaryotes.[6] Ndh-II or NADH:quinone oxidoreductase II is a single-subunit protein present in microbes but not in human mitochondria. Ndh-I couples energy released by NADH oxidation to pumping protons, but Ndh-II only catalyzes oxidation of NADH and reduction of quinones without the ability to pump protons. In *E. coli*, there are three respiratory chain cytochrome oxidases: $Cytbo_3$ (CyoABCD), Cytbd-I (CydAB), and Cytbd-II (AppBC) and these enzymes are suggested to function under different conditions.[7,8] Since most cellular NADH is consumed in aerobic respiration, we hypothesized that mutating respiratory chain genes would likely alter the NADH/NAD^+ ratio.

To study the effects of NADH dehydrogenases on NADH/NAD^+ ratio, we individually knocked out the F-subunit of Ndh-I (Δ*nuoF*), Ndh-II (Δ*ndh*), and both together (Δ*nuoF*Δ*ndh*). The F-subunit of Ndh-I is directly involved in FMN-mediated oxidation of NADH.[33] The Δ*ndh* strain gave 3.1-fold higher reporter fluorescence relative to wild-type *E. coli* (Figure 3B). This is consistent with previous studies reporting Ndh-II as the predominant pathway for NADH oxidation in *E. coli*.[34,35] However, the reporter fluorescence of

DOI: 10.1021/acssynbio.8b00485
ACS Synth. Biol. 2019, 8, 264−273

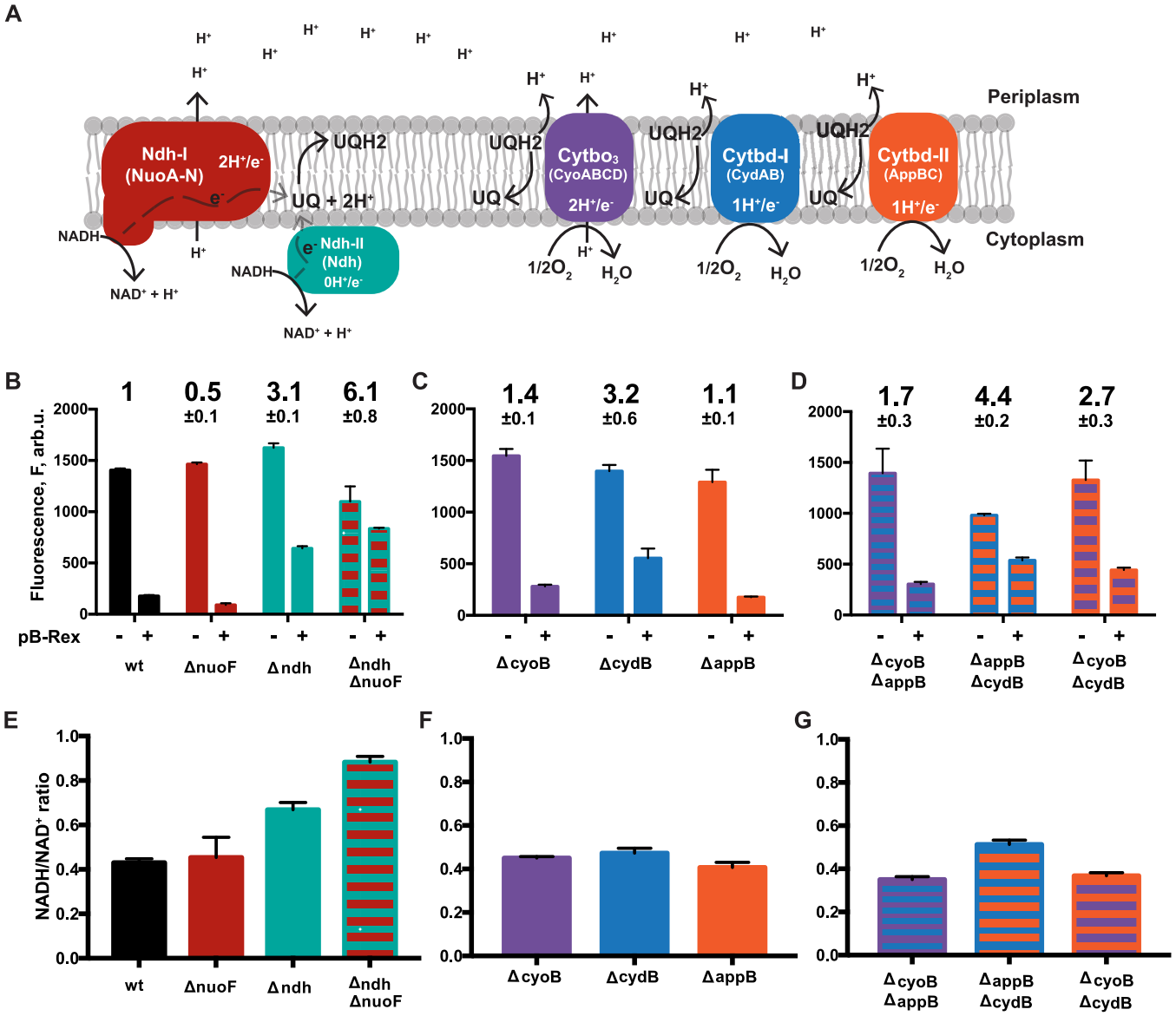

Figure 3. Redox state of respiratory chain mutants. (A) Illustration of respiratory chain enzymes embedded in the inner membrane of *E. coli*. Ndh-I and II are NADH dehydrogenases, and Cytbo3, Cytbd-I, and Cytbd-II are cytochrome oxidases. UQH2 and UQ are the reduced and oxidized forms of quinone. (B–D) GFP reporter fluorescence of wildtype and NADH-dehydrogenase mutants (B), cytochrome oxidase single mutants (C), and cytochrome oxidase double mutants (D). For each strain, the fluorescence of reporter only (pB-Rex-, left bar) and reporter with B-Rex (pB-Rex +, right bar) are shown. Numbers above bars represent fold change in biosensor-reporter fluorescence, relative to wildtype. *Y*-axis is normalized fluorescence units of GFP. (E–G) NADH/NAD+ ratio measured with enzymatic-kit based assay of wildtype and respiratory chain mutants in the same order as above. Error bar represents standard deviation of three replicates.

Δ*nuoF* strain was half of wild type *E. coli*. This result was unexpected, but consistently observed when experiments were repeated. However, without determining the lower sensitivity threshold of the biosensor, we may not know if that actual NADH/NAD$^+$ change is significant. One plausible mechanistic explanation based on studies by Calhoun et al., is that knocking out Ndh-I partially uncouples NADH oxidation from proton-pumping.[36] Therefore, to maintain the desired proton gradient, cells may increase NADH oxidation through Ndh-II, which might lead to the observed lower NADH/NAD$^+$ in the Δ*nuoF* strain. Higher Ndh-II activity would increase the quinol pool, allowing cytochrome oxidases to compensate loss of proton gradient. The double knockout Δ*nuoF*Δ*ndh* strain gave the highest reporter fluorescence (6.1-fold higher than wild type), reaching nearly the same level as a constitutively active reporter (Figure 3B). This indicates high accumulation of NADH as expected due to the loss of both NADH dehydrogenases (Figure 3B).

Next, to investigate the impact of cytochrome oxidases Cytbo$_3$ (*cyo*), Cytbd-I (*cyd*), and Cytbd-II (*app*) on the NADH/NAD+ ratio, we generated single and double knock-outs of all three enzymes by knocking out the heme-binding subunits CyoB, AppB, CydB of these cytochrome oxidases. Although we could knock out all three cytochrome oxidases under anaerobic conditions, the cells could not grow aerobically which is consistent with a previous study.[37] Reporter fluorescence of Δ*cyoB* and Δ*appB* strains were comparable to wild type, but Δ*cydB* strain showed 3.2-times greater fluorescence than wild type (Figure 3C). Among the double knockouts, reporter fluorescence of Δ*cyoB*Δ*appB* was

DOI: 10.1021/acssynbio.8b00485
ACS Synth. Biol. 2019, 8, 264–273

modestly higher (1.7-times) than wild type. However, both double mutants lacking *cydB* (Δ*appB*Δ*cydB* and Δ*cyoB*Δ*cydB*) gave 4.4- and 2.7-fold greater reporter fluorescence than wild type, respectively (Figure 3D). Proton-pumping Cytbo$_3$ (*cyo*) is thought to be the major quinol oxidase under aerobic condition, expressed at a level ∼300 molecules per cell.[38] Cytochrome bd-I (*cydB*) is induced under microaerobic and anaerobic conditions, but is also expressed at a comparable amount ∼200 molecules per cell.[38] Our results show that knocking out Cytbd-I in aerobically grown cells significantly increases the NADH/NAD$^+$ redox ratio suggesting Cytbd-I could play an important role in maintaining redox balance through quinol oxidation even in aerobic conditions. Why *E. coli* harbors three cytochrome oxidases and the redundancy built into the bacteria respiratory chain is not fully understood. It is apparent from our results that one cytochrome oxidase is sufficient to maintain the redox state in standard laboratory growth conditions using oxygen as an electron acceptor. Growth under different conditions could possibly reveal a greater dependency on each individual cytochrome oxidase.

We validated the biosensor-reporter measurements independently for all strains using a commercial enzyme-based NAD(H) quantification system. We found that the results from both methods were in broad agreement (Figure 3E−G, described in the methods section) except for the Δ*cydB* and Δ*nuoF* strains. The redox states of these strains were closer to wild type than estimated by the biosensor-reporter. Discrepancy may arise due to reduced sensitivity of the enzyme-based assay caused by a relatively high baseline at low NADH/NAD$^+$ levels. However, NADH/NAD$^+$ trends determined by the enzymatic assay were generally consistent with reporter fluorescence. We note that the biosensor is useful for comparing relative differences in NADH/NAD$^+$ because a change in reporter fluorescence is proportional to the NADH/NAD$^+$ ratio, but the numerical value of the fold change in the reporter may not be the same as the fold change in NADH/NAD$^+$. Quantitative comparisons of NADH/NAD$^+$ based on reporter fluorescence requires a calibration curve, which would be hard to establish due to challenges with exogenous supplementation of NADH in the growth medium (rapid oxidation and poor transport). However, with advances in cell-free platforms for transcription-based reporting, this may soon be possible.

Redox State in *E. coli* Grown under Different Carbon Sources. *E. coli* is well-known for its flexible metabolism, which allows it to grow on different nutrition sources. Since each source activates metabolic pathways with different redox demands, we wanted to use the biosensor-reporter to measure NADH/NAD$^+$ levels in *E. coli* cells grown aerobically with several common carbon sources. We tested glucose (as a reference), glycerol, pyruvate, glycerol, acetate, xylose, and succinate. Glycerol, pyruvate, and lactate feed directly into glycolysis, succinate is an important TCA cycle intermediate; xylose is a five-carbon sugar metabolized through pentose phosphate pathway before entering glycolysis. Acetate metabolism is more complex requiring the glyoxylate shunt along with other essential pathways to support growth. We observed that reporter fluorescence in nearly all carbon sources was slightly below that of glucose (Figure 4) suggesting that NADH/NAD$^+$ is modestly altered by changing carbon source. However, cells grown on acetate gave 2.5-times higher reporter fluorescence than glucose. This result is consistent with a detailed metabolomic study by Bennett et al. in which *E. coli*

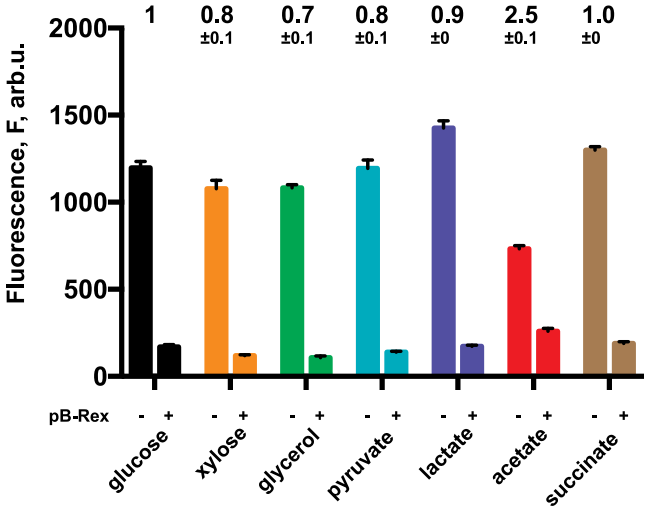

Figure 4. Redox state of wildtype *E. coli* grown on different carbon sources. Fluorescence of reporter only (pB-Rex-, left) and reporter with B-Rex (pB-Rex+, right bar) is shown. Numbers above bars represent fold change in biosensor-reporter fluorescence relative to cells grown in glucose. *Y*-axis is normalized fluorescence units of GFP. Error bar represents standard deviation of three replicates.

grown on acetate exhibited an NADH/NAD$^+$ ratio twice that of glucose: ∼0.055 in acetate compared to ∼0.03 in glucose.[16] Acetate is a fermentation product of *E. coli* that can be secreted at elevated intracellular NADH/NAD$^+$ when glucose uptake surpasses the metabolic capacity of the cells in aerobic growth.[34] Acetate is also known to cause global stress responses and inhibit cell growth.[39,40] It is unclear if the elevated NADH/NAD$^+$ we observe is required to assimilate acetate for growth or is a result of a stress response caused by acetate.

Redox Biosensor-Reporter System as a Tool for High-Throughput Screening. Engineering microbes for production of fuels and chemicals has largely focused on optimizing enzyme levels to facilitate high carbon flux through a desired pathway. However, the cofactor ratio is increasingly recognized as an major bottleneck because altering the ratio of reduced to oxidized forms can provide the thermodynamic driving force for less favorable reactions.[41,42] For instance, the availability of excess reducing equivalents improved *n*-butanol productivity to a very high yield.[43] High-throughput screening is a powerful tool for identifying strain backgrounds with altered NADH/NAD$^+$ pool, a task that can otherwise be very difficult by conventional analytical methods. Biosensors have been used with great success to evolve and engineer microbes by high-throughput screening.

To evaluate if our redox biosensor-reporter could be used for screening, we sought to enrich *E. coli* mutants with high NADH/NAD+ from a mixed population with wild-type *E. coli*. To mimic a library of mutants with varying proportions of high NADH variants, we mixed wild-type *E. coli* with either Δ*ndh* or Δ*cydB*Δ*appB* mutants in the following proportions: 1:1, 10:1, 1,000:1, 10,000:1. Δ*ndh* and Δ*cydB*Δ*appB* strains gave 3.1- and 4.4-fold higher NADH/NAD+ signal, respectively, compared to wildtype (Figure 3B,D). Using fluorescence activated cell sorting, we sorted the top 5% fluorescent cells from each mixture, plated them, and genotyped 30 randomly chosen clones as wildtype or mutant by PCR. For higher dilutions (100:1 to 10,000:1 of mutant to wild-type *E. coli*), the

DOI: 10.1021/acssynbio.8b00485
ACS Synth. Biol. 2019, 8, 264−273

sorted samples were grown to exponential phase and the top 5% fluorescent cells of the regrown sample were sorted again, followed by plating and colony PCR. Our results show that even at the highest proportion of wildtype to mutant (10 000:1) nearly 80% of the clones after enrichment were mutants (Figure 5). This result suggests that the redox biosensor-reporter can be used to screen medium-sized pooled libraries containing up to 10^4 variants.

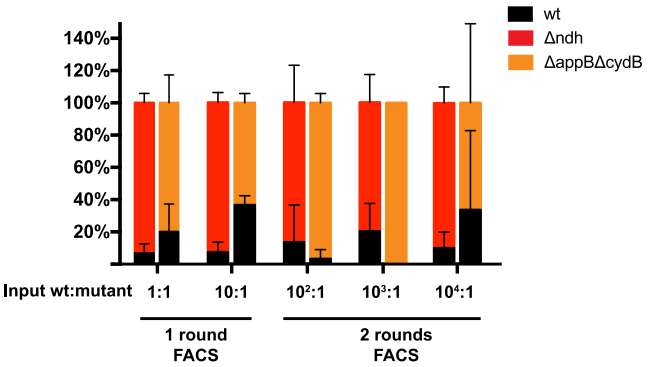

Figure 5. Evaluation of B-Rex biosensor-reporter as a high-throughput screening tool. *X*-axis is the proportion of wildtype to mutant in the starting population. *Y*-axis is the proportion of wildtype to mutant by PCR genotyping 30 colonies after enrichment using fluorescence-activated cell sorting. Black, red, and orange bars denote wildtype, and Δ*ndh* mutant and Δ*appB*Δ*cydB* double mutant, respectively.

The large error in the 10 000:1 wildtype-to-Δ*cydB*Δ*appB* test suggests that we may be close to the limit of detection of the biosensor-reporter. To assess if the mutants have a growth advantage over wild type, we measured the growth rate of all three strains individually in a plate reader. We found that the mutants grew slower than wild type and were therefore, if anything, at a minor growth disadvantage (Supplementary Figure S2). It is important to note that since regrowth of sorted cells may distort the population distribution, the fraction of mutants recovered after sorting may be confounded by artifacts due to sorting. In summary, the redox biosensor-reporter can be used to screen medium-sized strain libraries containing up to 10^4 variants for altered NADH capacity. More sensitive screens can be carried out by enhancing the dynamic range of the biosensor-reporter by further promoter engineering and/or by additional rounds of enrichment by cell sorting.

DISCUSSION

In this study, we constructed and validated a redox biosensor system based on transcription repressor Rex for accurate, noninvasive measurement of NADH/NAD^+ ratio in bacteria. We employed structural models of Rex bound to DNA to evaluate the binding affinities of different operator sites. By placing operator sites of varying affinities within a constitutive *E. coli* promoter, we showed that the dynamic range and maximum reporter signal of Rex can be optimized to make it a useful regulatory biosensor. The Rex biosensor coupled to a reporter proved to be an effective tool to screen variant libraries based on redox and could also enable dynamic control of metabolic pathways in response to intracellular redox changes. Since Rex is a repressor, it could be ported to nonmodel bacteria with a known constitutive promoter for redox sensing by optimizing the placement of its operator site. Rex-based biosensors could potentially be used in eukaryotes by fusing to the Rex protein domains that activate or repress transcription[44] (*e.g.*,VP16 or KRAB) or that modify the epigenetic state in response to redox changes.

The redox differences we observed in the respiratory chain mutants highlight the complex underlying relationship between cofactor metabolism, cellular redox, and respiration. When Ndh-I is knocked out, the NADH oxidation step may be uncoupled from proton-pumping, resulting in a loss of proton gradient in the first half of the respiratory chain. To maintain the desired proton gradient for numerous cellular processes, cells may upregulate NADH oxidation to reduce more quinone to allow cytochrome oxidases to compensate the loss of proton gradient. Calhoun et al. observed increased NADH-coenzyme Q1 reductase activity in membrane extracts from an Ndh-I deletion (Δ*nuoF*) strain besides wild-type, suggesting an upregulation in NADH oxidation in the Ndh-I mutant.[36] They also found that when Ndh-I and -II were knocked out, the NADH oxidation in membrane extracts was fully abolished, which is consistent with our observation of the highest NADH/NAD^+ in Δ*nuoF*Δ*ndh* double mutant. Under surplus nutrition, as is the case in our glucose-unlimited media experiments, although both Ndh-I and Ndh-II may be active, the uncoupled NADH dehydrogenase Ndh-II may be dominant because cells need to counteract increasing NADH/NAD+ triggered by faster metabolism. As glucose uptake increases, *E. coli* is reported to upregulate Ndh-II expression more than Ndh-I expression to compensate for increasing NADH/NAD^+.[34] This could be because proton-coupled NADH dehydrogenase Ndh-I is calibrated to oxidize NADH to maintain the right proton motive force required for ATP synthesis. In contrast, under glucose-limiting conditions, it was observed that knocking out Ndh-II (Δ*ndh*) had only a small effect on respiration, leading to the conclusion that Ndh-I is the main driver of NADH oxidation.[45] On the basis of our results and on these previous reports, we speculate that cells might adjust NADH oxidation through Ndh-I and Ndh-II under different growth conditions. When the carbon source is unlimited, Ndh-II oxidizes excess NADH to support redox balance and fast growth, and when the favored carbon source such as glucose becomes limited, cells may increase energy efficiency to favor NADH oxidation by Ndh-I as a mechanism to conserve energy and generate a proton based force for ATP synthesis. The redox biosensor could be useful tool to gain a deeper mechanistic understanding of the complex genetic and environmental causes affecting cellular redox.

High-throughput redox screening has the potential utility to increase understanding of microbial metabolism with applications in both medicine and biotechnology. Linking redox changes to mutations on a genome-wide scale would provide a comprehensive genotype-phenotype metabolic map of an organism, leading to a better understanding of redox flow and metabolism. Traditional genome-wide screens generally require a life or death selection to enrich or deplete mutants with the desired phenotype. However, redox changes cannot easily be tied directly to cell survival. A redox biosensor can enable genome-wide screening by sorting and deep sequencing barcoded mutant libraries into fluorescent bins. Microbial screens using the Rex biosensor could be used in several applications. A genome-wide redox screen could identify mutations that perturb the redox state and affect cell viability, leading to valuable insight into new mechanisms by which antibiotic resistance may emerge. Kohanski et al. showed that

DOI: 10.1021/acssynbio.8b00485
ACS Synth. Biol. 2019, 8, 264−273

bactericidal antibiotics, such as gyrase or peptidoglycan inhibitors, kill by a common hydroxyl radical mechanism mediated by a large drop in the NADH/NAD$^+$ ratio, and knocking out the TCA cycle genes to throttle the NADH level reduces antibiotic susceptibility.[46] Engineering microbes for producing biofuels or other highly reduced compounds requires excess NADH reducing equivalents to provide the required driving force.[43] Since cells tolerate only a narrow margin of redox imbalance, the lack of reducing power from the cell's native metabolic capacity is often a limitation in pathway optimization. Using the redox biosensor, we can evolve a microbe, through rounds of genome-wide mutagenesis and selection, toward higher reducing capacity, together with a "sink" reaction to consume NADH to maintain overall redox balance.

MATERIALS AND METHODS

Materials. Q5 HiFi DNA polymerase, OneTaq DNA polymerase, and NEBuilder HiFi DNA assembly mix were purchased from New England Biolabs. Wizard plus SV Minipreps DNA Purification System and NAD/NADH-Glo Assays were purchased from Promega. NADH and NAD were purchased from Roche. MOPS minimal buffer (5×) was purchased from Teknova.

Structural Comparison of Rex Operators. Structural analysis was based on *Thermus aquaticus* Rex (PDB: 3IKT) using Pymol. For visualizing Rex interaction with the operator, the DNA sequence was modeled in using 3DNA[47] and then visualized with Pymol.

Strains and Growth Conditions. All strains used in this study were derivatives of *E. coli* K12 RL3000 (see Table S1).[48] Respiratory chain mutants of RL3000 were constructed with P1 transduction using Keio collection, followed by marker removal by PCP20 plasmid. Overnight cultures of wildtype or mutants grown in LB were inoculated into MOPS minimal media with glucose or other carbon sources at a starting OD600 of ~0.05. To compare biosensor-reporter induction in anaerobic condition vs aerobic conditions, cells were cultured with MOPS minimal media with 20 mM glucose. The RL3000 wild-type strain was grown well aerated in 5 mL of media in 125 mL flasks, and shaken at 250 rpm for aerobic growth. RL3000 was cultured in 5 mL of media in 125 mL flasks, stirred by magnetic bars in an anaerobic chamber for anaerobic growth. MOPS minimal media with 20 mM glucose was used in the study of wildtype and respiratory chain mutants. For studying effects of carbon sources, MOPS minimal media with 20 mM glucose was used as a reference; concentrations of other carbon sources were adjusted to match the same mole of carbons as glucose (for example, 40 mM glycerol), and cells were grown aerobically as described above.

Plasmids Construction. All plasmids and primers are listed in Table S2. Q5 HiFi DNA polymerase (NEB) was used for PCR. Plasmids were constructed using Gibson Assembly with gel purified PCR products. After chemically competent *E. coli* DH5α was transformed with Gibson assembly products, cells were recovered and plated on LB plates with corresponding antibiotics. Plasmids from single colonies were harvested after overnight growth with antibiotics and sequenced for validating the clone (Quintarabio Biosciences).

Plasmid pB-Rex was constructed by amplifying the B-Rex gene from *B. subtilis* genomic DNA and cloned into pBBR1-MCS5 under the control of synthetic promoter apFAB338 (gnR)[49] (see Supporting Information for plasmid map). Plasmids pROP-PP and -IP reporters were derivatives of a plasmid with pSC101 origin of replication containing spectinomycin resistance cassette.[29] Additionally, a constitutively expressing mCherry was amplified from pJ251-GERC (a gift from George Church Addgene plasmid no. 47441) and inserted into the reporter plasmids (pROP-PP and -IP) to serve as a control for normalization for aerobic experiments. FMN-based fluorescent protein (FbFP) was amplified from pBAsyn[48] and assembled with pROP-PP and -IP reporters (see Supporting Information for plasmid maps). GFP was used as reporter in pROP-IP in the study of respiratory chain mutants (see Supporting Information for plasmid map). The ribosome binding Site (RBS) sequence was designed using the Salis RBS calculator.[50]

Fluorescence Normalization. Cells were grown to an OD600-0.5 before fluorescence was measured in a Tecan M200 plate reader. The excitation and emission wavelengths used for measuring FbFP, GFP, and mCherry are 450 nm/490 nm, 488 nm/530 nm and 580 nm/625 nm, respectively. FbFP fluorescence for comparison of aerobic and anaerobic conditions was normalized by cell density (OD600), and GFP fluorescence for investigating respiratory chain mutants and effects of carbon sources was additionally normalized by mCherry fluorescence. For the experiment investigating effects of carbon sources, fluorescence was normialized to wild-type strain grown in glucose.

Quantification of NAD$^+$ and NADH in Different Strains. NAD$^+$ and NADH quantifications were performed according to the NAD/NADH glo assay protocol from Promega. *E. coli* strains were grown to OD ~ 0.5 aerobically in flask or anaerobically in anaerobic chamber as described before. A 1 mL sampling of cells was spun down and resuspended in 200 μL of phosphate-buffered saline; 50 μL of cell suspension was then added to a 96 well plate. Then 50 μL of lysis buffer (0.2 M NaOH and 1% DTAB) was added to the cell suspension to lyse the cells. To measure NADH, 50 μL of the lysed cell suspension was incubated at 60 °C for 15 min. Then 50 μL of Trizma/HCl solution (mixing 0.4 M HCl and 0.5 M Trizma base) was added to the base treated cell suspension after it was cooled to room temperature for 10 min. To measure NAD$^+$, 25 μL of 0.4 M HCl was added to 50 μL of lysed cell suspension, and the mixture was then incubated at 60 °C for 15 min. After the treatment, 25 μL of Trizma base was added to the acid treated cell suspension, and the mixture was cooled to room temperature for 10 min. Finally, 50 μL of NAD/NADH-Glo Detection Reagent was mixed with 50 μL of the treated cell suspension in a 96 well plate, the mixture was incubated at room temperature, and the luminescence was measured at 5 min intervals in the Tecan M200 plate reader. A 50 μL sampling of NAD$^+$ and NADH standards (ranging from 0 to 400 nM) was prepared and mixed with 50 μL of NAD/NADH-Glo Detection Reagents. The standard curves were generated and measured at the same time as the samples. The concentrations of NAD$^+$ and NADH of each *E. coli* strain were calculated based on the standard curves of NAD$^+$ and NADH. The ratios of NADH and NAD$^+$ are reported.

Fluorescence Activated Cell Sorting (FACS). We used SONY LE-SH800 for cell sorting. All the experiments were performed with biological triplicates. Δ*ndh* and wild-type strains containing both pROP-IP and pB-Rex plasmids were grown to OD600-0.5−0.6. Wild-type and Δ*ndh* were adjusted to similar cell densities and then mixed with a ratio of wild-type/Δ*ndh* at 1:1, 10:1, 100:1, 1000:1, and 10 000:1. The same

DOI: 10.1021/acssynbio.8b00485
ACS Synth. Biol. 2019, 8, 264−273

procedure was carried for mixing Δ*appB*Δ*cydB* with wild-type. During the cell sorting procedure, the top 5% of the population of each mixture was sorted, and the sorted cells were then recovered in SOB for 2 h. Cells mixed at ratios of 1:1 and 10:1 were recovered after sorting and plated on LB plates with corresponding antibiotics. Cells mixed at ratios higher than 10:1 were recovered after sorting and cultured in 5 mL of MOPS minimal with 20 mM glucose and grown aerobically as described earlier. The top 5% population of the regrown cultures were sorted again, recovered in SOB, and plated on LB plates with corresponding antibiotics. To estimate the percentage of mutant cells after sorting, 10 colonies were checked by PCR (3 replicates) using OneTaq DNA polymerase. PCR products from mutants had a distinct size from wild-type. High NADH mutant recovery was calculated as the fraction of mutants divided among all colonies tested. Average and standard deviation of the recovery were then calculated from biological triplicates. Enrichment was calculated by multiplying the recovery by the corresponding mixing ratio.

■ ASSOCIATED CONTENT

Supporting Information

The Supporting Information is available free of charge on the ACS Publications website at DOI: 10.1021/acssynbio.8b00485.

Strains and plasmids; primers for constructin plasmids; structure and sequence alignment of T-Rex and B-Rex DNA binding domain (DBD); growth comparison of wild-type, *Dndh*, *DappBDcydB* strains; plasmid maps for reporters plasmids and pB-Rex plasmid used in this study (PDF)

■ AUTHOR INFORMATION

Corresponding Author

*E-mail: sraman4@wisc.edu.

ORCID

Srivatsan Raman: 0000-0003-2461-1589

Author Contributions

Y.L., R.L., and S.R conceived the study. Y.L and S.R designed experiments. Y.L performed experiments. Y.L., R.L., and S.R analyzed the data. Y.L., R.L., and S.R wrote the manuscript.

Notes

The authors declare the following competing financial interest(s): The authors have filed a provisional patent application on this technology.

Plasmids generated in this study are available from Addgene Inc.

■ ACKNOWLEDGMENTS

This work was funded by the DOE Great Lakes Bioenergy Research Center (DOE BER Office of Science DE-FC02-07ER64494). We thank Dr. Jennifer Reed for advice on respiratory chain mutants. We thank Dr. Michaela TerAvest for critical review of the manuscript.

■ REFERENCES

(1) Eto, K., Tsubamoto, Y., Terauchi, Y., Sugiyama, T., Kishimoto, T., Takahashi, N., Yamauchi, N., Kubota, N., Murayama, S., Aizawa, T., et al. (1999) Role of NADH Shuttle System in Glucose-Induced Activation of Mitochondrial Metabolism and Insulin Secretion. *Science (Washington, DC, U. S.) 283* (5404), 981−985.

(2) Lehninger, A., Nelson, D. L., and Cox, M. M. (2008) *Lehninger Principles of Biochemistry*, W. H. Freeman.

(3) Koch-Nolte, F., Haag, F., Guse, A. H., Lund, F., and Ziegler, M. (2009) Emerging Roles of NAD+ and Its Metabolites in Cell Signaling. *Sci. Signaling 2*, mr1.

(4) Santidrian, A. F., Matsuno-yagi, A., Ritland, M., Seo, B. B., Leboeuf, S. E., Gay, L. J., Yagi, T., and Felding-habermann, B. (2013) Mitochondrial Complex I Activity and NAD + /NADH Balance Regulate Breast Cancer Progression. *J. Clin. Invest. 123* (3), 1068−1081.

(5) Forster, A. H., and Gescher, J. (2014) Metabolic Engineering of Escherichia Coli for Production of Mixed-Acid Fermentation End Products. *Front. Bioeng. Biotechnol. 2* (May), 16.

(6) Friedrich, T., and Scheide, D. (2000) The Respiratory Complex I of Bacteria, Archaea and Eukarya and Its Module Common with Membrane-Bound Multisubunit Hydrogenases. *FEBS Lett. 479*, 1−5.

(7) Borisov, V. B., Murali, R., Verkhovskaya, M. L., Bloch, D. A., Han, H., Gennis, R. B., and Verkhovsky, M. I. (2011) Aerobic Respiratory Chain of Escherichia Coli Is Not Allowed to Work in Fully Uncoupled Mode. *Proc. Natl. Acad. Sci. U. S. A. 108* (42), 17320−17324.

(8) Borisov, V. B., Gennis, R. B., Hemp, J., and Verkhovsky, M. I. (2011) The Cytochrome Bd Respiratory Oxygen Reductases. *Biochim. Biophys. Acta, Bioenerg. 1807*, 1398−1413.

(9) Shepherd, M., Sanguinetti, G., Cook, G. M., and Poole, R. K. (2010) Compensations for Diminished Terminal Oxidase Activity in Escherichia Coli: Cytochrome Bd-II-Mediated Respiration and Glutamate Metabolism. *J. Biol. Chem. 285* (24), 18464−18472.

(10) Brøndsted, L., and Atlung, T. (1996) Effect of Growth Conditions on Expression of the Acid Phosphatase (Cyx-AppA) Operon and the AppY Gene, Which Encodes a Transcriptional Activator of Escherichia Coli. *J. Bacteriol. 178* (6), 1556−1564.

(11) Holm, A. K., Blank, L. M., Oldiges, M., Schmid, A., Solem, C., Jensen, P. R., and Vemuri, G. N. (2010) Metabolic and Transcriptional Response to Cofactor Perturbations in Escherichia Coli. *J. Biol. Chem. 285* (23), 17498−17506.

(12) Miyawaki, A., Llopis, J., Heim, R., Mccaffery, J. M., Adams, J. a., Ikurak, M., and Tsien, R. Y. (1997) Letters to Nature Fluorescent Indicators for Ca 2 + Based on Green Fluorescent Proteins and Calmodulin. *Nature 388*, 882−887.

(13) Nausch, L. W. M., Ledoux, J., Bonev, A. D., Nelson, M. T., and Dostmann, W. R. (2008) Differential Patterning of CGMP in Vascular Smooth Muscle Cells Revealed by Single GFP-Linked Biosensors. *Proc. Natl. Acad. Sci. U. S. A. 105* (1), 365−370.

(14) Imamura, H., Huynh Nhat, K. P., Togawa, H., Saito, K., Iino, R., Kato-Yamada, Y., Nagai, T., and Noji, H. (2009) Visualization of ATP Levels inside Single Living Cells with Fluorescence Resonance Energy Transfer-Based. *Proc. Natl. Acad. Sci. U. S. A. 106* (37), 15651−15656.

(15) Belousov, V. V., Fradkov, A. F., Lukyanov, K. A., Staroverov, D. B., Shakhbazov, K. S., Terskikh, A. V., and Lukyanov, S. (2006) Genetically Encoded Fluorescent Indicator for Intracellular Hydrogen Peroxide. *Nat. Methods 3* (4), 281−286.

(16) Bennett, B. D., Kimball, E. H., Gao, M., Osterhout, R., van Dien, S. J., and Rabinowitz, J. D. (2009) Absolute Metabolite Concentrations and Implied Enzyme Active Site Occupancy in Escherichia Coli. *Nat. Chem. Biol. 5* (8), 593−599.

(17) Vidugiriene, J., Leippe, D., Sobol, M., Vidugiris, G., Zhou, W., Meisenheimer, P., Gautam, P., Wennerberg, K., and Cali, J. J. (2014) Bioluminescent Cell-Based NAD(P)/NAD(P)H Assays for Rapid Dinucleotide Measurement and Inhibitor Screening. *Assay Drug Dev. Technol. 12* (9−10), 514−526.

(18) Blacker, T. S., and Duchen, M. R. (2016) Investigating Mitochondrial Redox State Using NADH and NADPH Autofluorescence. *Free Radical Biol. Med. 100*, 53−65.

(19) De Graef, M. R., Alexeeva, S., Snoep, J. L., and Teixeira De Mattos, M. J. (1999) The Steady-State Internal Redox State (NADH/NAD) Reflects the External Redox State and Is Correlated with

DOI: 10.1021/acssynbio.8b00485
ACS Synth. Biol. 2019, 8, 264−273

Catabolic Adaptation in Escherichia Coli. *J. Bacteriol. 181* (8), 2351−2357.
(20) Brekasis, D., and Paget, B. (2003) A Novel Sensor of NADH/NAD+ Redox Poise in Streptomyces Coelicolor A3 (2). *EMBO J. 22*, 4856.
(21) Wang, E., Bauer, M. C., Rogstam, A., Linse, S., Logan, D. T., and Von Wachenfeldt, C. (2008) Structure and Functional Properties of the Bacillus Subtilis Transcriptional Repressor Rex. *Mol. Microbiol. 69* (2), 466−478.
(22) Hung, Y. P., Albeck, J. G., Tantama, M., and Yellen, G. (2011) Imaging Cytosolic NADH-NAD+ Redox State with a Genetically Encoded Fluorescent Biosensor. *Cell Metab. 14*, 545.
(23) Zhao, Y., Jin, J., Hu, Q., Zhou, H. M., Yi, J., Yu, Z., Xu, L., Wang, X., Yang, Y., and Loscalzo, J. (2011) Genetically Encoded Fluorescent Sensors for Intracellular NADH Detection. *Cell Metab. 14* (4), 555−566.
(24) Zhao, Y., Hu, Q., Cheng, F., Su, N., Wang, A., Zou, Y., Hu, H., Chen, X., Zhou, H.-M., Huang, X., et al. (2015) SoNar, a Highly Responsive NAD+/NADH Sensor, Allows High-Throughput Metabolic Screening of Anti-Tumor Agents. *Cell Metab. 21* (5), 777−789.
(25) Dietrich, J. A., Shis, D. L., Alikhani, A., and Keasling, J. D. (2013) Transcription Factor-Based Screens and Synthetic Selections for Microbial Small-Molecule Biosynthesis. *ACS Synth. Biol. 2* (1), 47−58.
(26) Raman, S., Rogers, J. K., Taylor, N. D., and Church, G. M. (2014) Evolution-Guided Optimization of Biosynthetic Pathways. *Proc. Natl. Acad. Sci. U. S. A. 111* (50), 17803.
(27) Zhang, F., Carothers, J. M., and Keasling, J. D. (2012) Design of a Dynamic Sensor-Regulator System for Production of Chemicals and Fuels Derived from Fatty Acids. *Nat. Biotechnol. 30* (4), 354−359.
(28) Tang, S.-Y., Qian, S., Akinterinwa, O., Frei, C. S., Gredell, J. A., and Cirino, P. C. (2013) Screening for Enhanced Triacetic Acid Lactone Production by Recombinant Escherichia Coli Expressing a Designed Triacetic Acid Lactone Reporter. *J. Am. Chem. Soc. 135* (27), 10099−10103.
(29) Rogers, J. K., Guzman, C. D., Taylor, N. D., Raman, S., Anderson, K., and Church, G. M. (2015) Synthetic Biosensors for Precise Gene Control and Real-Time Monitoring of Metabolites. *Nucleic Acids Res. 43* (15), 7648−7660.
(30) Zhang, J., Sonnenschein, N., Pihl, T. P. B., Pedersen, K. R., Jensen, M. K., and Keasling, J. D. (2016) Engineering an NADPH/NADP $^{+}$ Redox Biosensor in Yeast. *ACS Synth. Biol. 5* (12), 1546−1556.
(31) McLaughlin, K. J., Strain-Damerell, C. M., Xie, K., Brekasis, D., Soares, A. S., Paget, M. S. B., and Kielkopf, C. L. (2010) Structural Basis for NADH/NAD+ Redox Sensing by a Rex Family Repressor. *Mol. Cell 38*, 563.
(32) Walter, J., Hausmann, S., Drepper, T., Puls, M., Eggert, T., and Dihné, M. (2012) Flavin Mononucleotide-Based Fluorescent Proteins Function in Mammalian Cells without Oxygen Requirement. *PLoS One 7* (9), e43921.
(33) Friedrich, T., Dekovic, D. K., and Burschel, S. (2016) Assembly of the Escherichia Coli NADH:Ubiquinone Oxidoreductase (Respiratory Complex I). *Biochim. Biophys. Acta, Bioenerg. 1857* (3), 214−223.
(34) Vemuri, G. N., Altman, E., Sangurdekar, D. P., Khodursky, A. B., and Eiteman, M. A. (2006) Overflow Metabolism in Escherichia Coli during Steady-State Growth: Transcriptional Regulation and Effect of the Redox Ratio. *Appl. Environ. Microbiol. 72* (5), 3653−3661.
(35) Tran, Q. H., Bongaerts, J., Vlad, D., and Unden, G. (1997) Requirement for the Proton-Pumping NADH Dehydrogenase I of Escherichia Coli in Respiration of NADH to Fumarate and Its Bioenergetic Implications. *Eur. J. Biochem. 244* (1), 155−160.
(36) Calhoun, M. W., and Gennis, R. B. (1993) Demonstration of Separate Genetic Loci Encoding Distinct Membrane-Bound Respiratory NADH Dehydrogenases in Escherichia Coli. *J. Bacteriol. 175* (10), 3013−3019.
(37) Portnoy, V. A., Herrgård, M. J., and Palsson, B. Ø. (2008) Aerobic Fermentation of D-Glucose by an Evolved Cytochrome Oxidase-Deficient Escherichia Coli Strain. *Appl. Environ. Microbiol. 74* (24), 7561−7569.
(38) Cotter, P. A., Chepuri, V., Gennis, R. B., and Gunsalus, R. P. (1990) Cytochrome o (CyoABCDE) and d (CydAB) Oxidase Gene Expression in Escherichia Coli Is Regulated by Oxygen, PH and the Fnr Gene Product. *J. Bacteriol. 172* (11), 6333−6338.
(39) Luli, G., and Strohl, W. (1990) Comparison of Growth, Acetate Production, and Acetate Inhibition of Escherichia Coli Strains in. *Appl. Environ. Microbiol. 56* (4), 1004−1011.
(40) Kirkpatrick, C., Maurer, L. M., Oyelakin, N. E., Yoncheva, Y. N., Maurer, R., and Slonczewski, J. L. (2001) Acetate and Formate Stress: Opposite Responses in the Proteome of Escherichia Coli. *J. Bacteriol. 183* (21), 6466−6477.
(41) Wang, Y., San, K. Y., and Bennett, G. N. (2013) Cofactor Engineering for Advancing Chemical Biotechnology. *Curr. Opin. Biotechnol. 24*, 994.
(42) Chen, X., Li, S., and Liu, L. (2014) *Trends Biotechnol. 32* (6), 337−343.
(43) Shen, C. R., Lan, E. I., Dekishima, Y., Baez, A., Cho, K. M., and Liao, J. C. (2011) Driving Forces Enable High-Titer Anaerobic 1-Butanol Synthesis in Escherichia Coli. *Appl. Environ. Microbiol. 77* (9), 2905−2915.
(44) Huang, G., Zhang, Y., Shan, Y., Yang, S., Chelliah, Y., Wang, H., and Takahashi, J. S. (2016) Circadian Oscillations of NADH Redox State Using a Heterologous Metabolic Sensor in Mammalian Cells. *J. Biol. Chem. 291*, 23906.
(45) Calhoun, M. W., Oden, K. L., Gennis, R. B., De Mattos, M. J. T., and Neijssel, O. M. (1993) Energetic Efficiency of Escherichia Coli: Effects of Mutations in Components of the Aerobic Respiratory Chain. *J. Bacteriol. 175* (10), 3020−3025.
(46) Kohanski, M. A., Dwyer, D. J., Hayete, B., Lawrence, C. A., and Collins, J. J. (2007) A Common Mechanism of Cellular Death Induced by Bactericidal Antibiotics. *Cell 130* (5), 797−810.
(47) Lu, X. J., and Olson, W. K. (2008) 3DNA: A Versatile, Integrated Software System for the Analysis, Rebuilding and Visualization of Three-Dimensional Nucleic-Acid Structures. *Nat. Protoc. 3*, 1213.
(48) Ghosh, I. N., and Landick, R. (2016) OptSSeq: High-Throughput Sequencing Readout of Growth Enrichment Defines Optimal Gene Expression Elements for Homoethanologenesis. *ACS Synth. Biol. 5*, 1519.
(49) Kovach, M. E., Elzer, P. H., Steven Hill, D., Robertson, G. T., Farris, M. A., Roop, R. M., and Peterson, K. M. (1995) Four New Derivatives of the Broad-Host-Range Cloning Vector PBBR1MCS, Carrying Different Antibiotic-Resistance Cassettes. *Gene 166*, 175.
(50) Salis, H. M., Mirsky, E. A., and Voigt, C. A. (2009) Automated Design of Synthetic Ribosome Binding Sites to Control Protein Expression. *Nat. Biotechnol. 27*, 946.

DOI: 10.1021/acssynbio.8b00485
ACS Synth. Biol. 2019, 8, 264−273